Myopic deconvolution of adaptive optics images by use of object and point-spread function power spectra

Jean-Marc Conan, Laurent M. Mugnier, Thierry Fusco, Vincent Michau, and Gérard Rousset

Adaptive optics systems provide a real-time compensation for atmospheric turbulence. However, the correction is often only partial, and a deconvolution is required for reaching the diffraction limit. The need for a regularized deconvolution is discussed, and such a deconvolution technique is presented. This technique incorporates a positivity constraint and some *a priori* knowledge of the object (an estimate of its local mean and a model for its power spectral density). This method is then extended to the case of an unknown point-spread function, still taking advantage of similar *a priori* information on the point-spread function. Deconvolution results are presented for both simulated and experimental data.

OCIS codes: 010.1080, 010.1330, 100.1830, 100.3020, 100.3190, 110.6770.

1. Introduction

The performance of high-resolution imaging with large optical instruments is severely limited by atmospheric turbulence. In the past 20 years various techniques have been proposed to overcome this limitation and to reach effectively the diffraction limit of telescopes. Speckle interferometry[1] was first proposed and is based on recording series of images with exposure times short enough to freeze the turbulence. Various numerical postprocessing methods[2–4] then permit the reconstruction of the observed object. Alternatively, adaptive optics[5,6] (AO) offers a real-time compensation for turbulence. One can therefore record long-exposure images without losing the object's high spatial frequencies that correspond to the fine details. The high spatial frequencies are not lost but they can, however, be severely attenuated since the correction is often only partial.[6–10] Consequently, the AO-corrected long-exposure images must be deconvolved to restore the object properly. A common feature of techniques for imaging through turbulence is that the point-spread function (PSF) is not known accurately, which makes deconvolution more difficult.

Our goal in this paper is to propose a deconvolution scheme based on a stochastic approach, which takes into account the noise in the image and the *a priori* information on the object to be restored, as well as the imprecise knowledge of the PSF.

The outline of the paper is as follows. The problem of the deconvolution of AO images is briefly presented in Section 2. Several approaches to this inverse problem are recalled in Section 3: minimum-mean-square error (MMSE) estimation, maximum *a posteriori* (MAP) estimation, and Wiener filtering. In Section 4, a regularized criterion to be minimized is derived from the *a posteriori* probability distribution, assuming that the PSF is known. The regularization function and the regularization parameter are both deduced from a model of the object's spatial power spectral density (PSD). The regularization issue, the use of additional positivity constraints, and the extension to a myopic deconvolution scheme are discussed and illustrated with numerical simulations. We use the term myopic deconvolution rather than blind deconvolution to underline the fact that the PSF is not completely unknown; indeed our scheme uses some available *a priori* information on the PSF, namely, its positivity and estimates of its ensemble mean and PSD. Finally, the deconvolution technique is applied to experimental data and the results are presented in Section 5.

The authors are with the Département d'Optique Théorique et Appliquée, Office National d'Études et de Recherches Aérospatiale, BP 72, F-92322 Châtillon Cedex, France.

Received 23 July 1997; revised manuscript received 6 November 1997.

0003-6935/98/214614-09$15.00/0

2. Framework: Partially Corrected Adaptive Optics Images

Within the isoplanatic angle, the intensity $i(r)$ at the focal plane of the system consisting of the atmosphere, the telescope, and the AO bench is given by

$$i(r) = h(r) * o(r) + n(r), \tag{1}$$

where r is the spatial coordinate, $o(r)$ is the observed object, $h(r)$ is the system PSF, and $n(r)$ is an additive zero-mean noise. In the sections below we consider that the object and the image are sampled on a regular grid; hence we have a vectorial formulation for Eq. (1):

$$\mathbf{i} = H\mathbf{o} + \mathbf{n}, \tag{2}$$

where $\mathbf{o}$, $\mathbf{i}$, and $\mathbf{n}$ are the vectors corresponding to the lexicographically ordered object, image, and noise, respectively. H is the Toeplitz[11] matrix corresponding to the convolution by the PSF h.

We consider here the case of AO-corrected long-exposure images. The AO correction is partial, and its quality depends on the observing conditions: turbulence strength, imaging wavelength, magnitude of the source used for wave-front sensing, and system characteristics.

The simulations presented in this paper are obtained under the following turbulence conditions: a Fried parameter[12] r_0 equal to 10 cm at the imaging wavelength 0.5 μm and a 10-m/s wind speed. We consider a 1.52-m telescope with a central obstruction diameter equal to 0.56 m. The AO system is equipped with a 10×10 piezostack mirror (of which 88 actuators are active). It uses a 9×9 subaperture Shack–Hartmann wave-front sensor, with 64 useful subapertures. The AO servoloop bandwidth is 80 Hz. With a tenth-magnitude guide star, the simulations give a Strehl ratio equal to 0.10 (intensity at the center of the field of the corrected long-exposure image normalized to the intensity at diffraction limit). The corresponding long-exposure optical transfer function (OTF) is shown in Fig. 1. This is a typical corrected OTF[7–10]: a low-frequency lobe and a high-frequency wing going up to the telescope cutoff frequency. The spatial frequencies between r_0/λ and D/λ, which would be lost without correction, are now preserved, although severely attenuated. The effect on the observation of astronomical objects is illustrated in Fig. 2. The figure shows the observed object, a tiny galaxy (4.2-arc sec field of view), and the corresponding long-exposure image deduced from Eq. (1). The fine details are blurred. The goal of the deconvolution is to correct for the OTF in order to restore the high spatial frequencies of the object properly. After a brief review of stochastic approaches in Section 3, several deconvolution schemes, which are applied to a noisy version of the image shown in Fig. 2, are presented and analyzed in Section 4.

3. Stochastic Approaches to the Restoration Problem

We consider in this section the problem of the deconvolution with a known PSF, which is called in this paper classical deconvolution. The extension to myopic deconvolution is discussed in Section 4.

It is now well known that the restoration of the object by use of the sole data is an unstable process (see in particular Refs. 13–15 and Refs. 16 and 17 for reviews). It is the case, for example, for the least-squares method[18] (minimization of $\|\mathbf{i} - \mathbf{o} * \mathbf{h}\|^2$), which corresponds to a maximum-likelihood (ML) solution in the case of white Gaussian noise. It is also the case with the Richardson–Lucy[19,20] algorithm, which corresponds to a ML solution in the case of Poisson noise. It is possible to regularize the solution by stopping the algorithm before convergence, but this leads to a poor control of the solution. It is instead preferable to modify the criterion to be minimized (or maximized), which corresponds to adding *a priori* information on the solution. The *a priori* information can be introduced either as a constraint (e.g., smoothness[18,21]) within a deterministic framework or through an *a priori* probability in a stochastic approach (see Ref. 17 for the link between the two approaches and Ref. 22 for a classification of the methods).

FIGURES

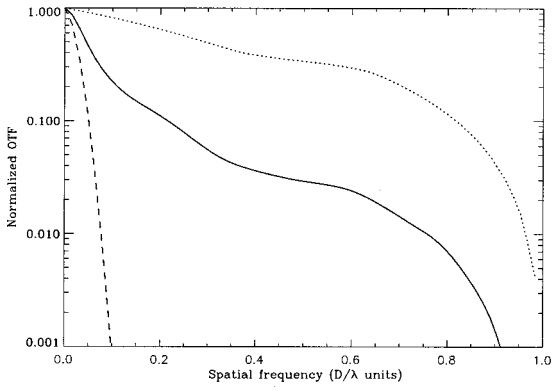

Fig. 1. Normalized OTF versus spatial frequency: AO-corrected OTF (solid curve). The aberration-free OTF (dotted curve) and the uncorrected OTF (dashed line) are shown for comparison. The spatial frequency is normalized to the telescope cutoff.

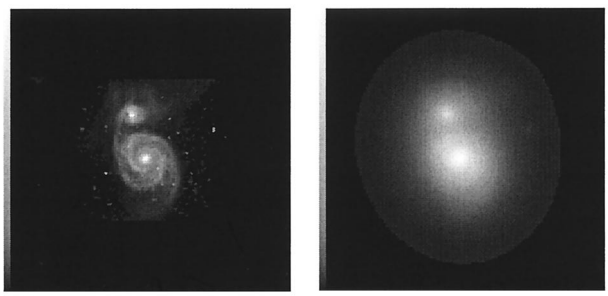

True Object (a) Corrected Image (b)

Fig. 2. (a) True object on 128×128 pixels, (b) AO-corrected image: simulation with Strehl ratio equal to 0.10, field of view 4.2 arc sec, wavelength 0.5 μm.

In stochastic approaches the object is seen as one realization of a stochastic process. The object is endowed with an *a priori* distribution $p(\mathbf{o})$, and Bayes' rule combines the likelihood of the data $p(\mathbf{i}|\mathbf{o})$ with this *a priori* distribution into the *a posteriori* probability distribution $p(\mathbf{o}|\mathbf{i})$:

$$p(\mathbf{o}|\mathbf{i}) \propto p(\mathbf{i}|\mathbf{o})p(\mathbf{o}). \tag{3}$$

This leads to two commonly used object estimation methods: the MAP estimation and the MMSE estimation. On the one hand, the MAP estimation defines the restored object as the most probable object, given the data:

$$\hat{\mathbf{o}}_{\text{map}} = \arg\max_{\mathbf{o}} p(\mathbf{o}|\mathbf{i}). \tag{4}$$

On the other hand, the MMSE estimator is defined as the one that minimizes, on average, the distance with the true object:

$$\hat{\mathbf{o}}_{\text{mmse}} = \arg\min_{\hat{\mathbf{o}}} E(\|\hat{\mathbf{o}} - \mathbf{o}\|^2), \tag{5}$$

where $E(\,)$ stands for the mathematical expectation with respect to the object and to the image noise. It can be shown that this estimator is the mean object with respect to the *a posteriori* probability distribution[23,24]:

$$\hat{\mathbf{o}}_{\text{mmse}} = E(\mathbf{o}|\mathbf{i}) = \int \mathbf{o}p(\mathbf{o}|\mathbf{i})\mathrm{d}\mathbf{o}. \tag{6}$$

In general, the calculation of the MMSE estimator is not tractable unless the estimator is assumed to be linear. The minimization of Eq. (5) under this assumption leads to the Wiener filter.[23,24] It is important to note that in the case of joint Gaussian statistics for the noise and the object, the Wiener, the MMSE, and the MAP estimators are identical.[23]

In Section 4 we use the MAP approach and show that this stochastic framework allows us to derive the regularization parameter from a reasonable model of the object spatial PSD. Note that, throughout this paper, the *a priori* statistics on the object are assumed to be Gaussian. This assumption can be justified by an information theory standpoint as being the least informative, given the first two moments of the *a priori* distribution. In contrast, deterministic methods leading to a regularized criterion usually use empirical regularizing functions (e.g., square norm of a Laplacian) to enforce the object smoothness.

4. Construction of a Regularized Criterion

A. Classical Deconvolution

1. *Maximum* a posteriori *Estimator with Gaussian Statistics*

We first consider the case of the classical deconvolution with Gaussian, zero-mean noise. This assumption of the noise allows us to obtain explicit expressions in Fourier space of the criteria to be minimized (for the classical and the myopic cases), as well as an analytic solution in Fourier space in the classical case. Yet, for astronomical imaging under low-light-level conditions or for objects of small extension, it is preferable to use a Poisson noise model instead (see Subsection 4.A.2).

With the above assumptions, the *a posteriori* probability distribution is easily derived:

$$\begin{aligned} p(\mathbf{o}|\mathbf{i}) &\propto p(\mathbf{i}|\mathbf{o})p(\mathbf{o}) \\ &\propto \exp[-1/2(\mathbf{i} - H\mathbf{o})^t R_n^{-1}(\mathbf{i} - H\mathbf{o})] \\ &\times \exp[-1/2(\mathbf{o} - \mathbf{o_m})^t R_o^{-1}(\mathbf{o} - \mathbf{o_m})], \end{aligned} \tag{7}$$

where we used the vectorial formulation introduced in Eq. (2) and the superscript t denotes transposition. R_o and R_n are the covariance matrices of the object and the noise, respectively, and $\mathbf{o_m} = E(\mathbf{o})$ is the mean object, that is, the ensemble mean of the class of objects being observed. Following Hunt,[25] we assume on the one hand that the mean object is not necessarily constant, so that $\mathbf{o}$ may not be stationary, which is closer to reality than the common stationarity assumption. On the other hand, in order to keep our problem tractable, we assume that $(\mathbf{o} - \mathbf{o_m})$ is stationary, so that the covariance matrix R_o is Toeplitz. Similarly, we assume that the noise is stationary, so that R_n is also Toeplitz; for a white noise (no correlation between pixels), this corresponds to considering that the variance of the noise remains uniform on the whole image.

The MAP estimation consists of maximizing $p(\mathbf{o}|\mathbf{i})$, which is equivalent to minimizing $-\ln[p(\mathbf{o}|\mathbf{i})]$; hence the following criterion:

$$J(\mathbf{o}) = (\mathbf{i} - H\mathbf{o})^t R_n^{-1}(\mathbf{i} - H\mathbf{o}) + (\mathbf{o} - \mathbf{o_m})^t R_o^{-1}(\mathbf{o} - \mathbf{o_m}), \tag{8}$$

to be minimized with respect to the object. The first term (least squares) corresponds to the likelihood, and the second term is the regularizing function.

Let us show that, with minor approximations, this criterion can be expressed in the Fourier domain as a function of the noise and the object spatial PSD's. It is well known that Toeplitz matrices can be approximated by circulant matrices,[17] with the approximation corresponding to a periodization. Within this approximation, the covariance matrices R_o and R_n and the convolution matrix H are diagonalized by a discrete Fourier transform[18] (DFT). One can therefore write

$$R_o = F^{-1}\,\text{diag}[\text{PSD}_o]F, \tag{9}$$

$$R_n = F^{-1}\,\text{diag}[\text{PSD}_n]F, \tag{10}$$

$$H = F^{-1}\,\text{diag}[\text{DFT}(h)]F, \tag{11}$$

where F is the two-dimensional DFT matrix, and $\text{diag}[x]$ denotes a diagonal matrix having x on its diagonal. PSD_o and PSD_n are the numerical power

spectral densities of the object and noise, respectively:

$$\begin{aligned}\mathrm{PSD}_o &= \mathrm{DFT}(E\{[\mathbf{o}(r') - \mathbf{o_m}(r')][\mathbf{o}(r'+r) - \mathbf{o_m}(r'+r)]\}) \\ &= E[|\tilde{\mathbf{o}}(f) - \tilde{\mathbf{o}}_\mathbf{m}(f)|^2] = E[|\tilde{\mathbf{o}}(f)|^2] - |\tilde{\mathbf{o}}_\mathbf{m}(f)|^2.\end{aligned} \tag{12}$$

Note that, following Jain,[11] we define the PSD of an image as the Fourier transform of its covariance, not of its autocorrelation (the latter being the common definition in signal processing). With Eqs. (9)–(11), a new expression of the criterion is deduced from Eq. (8):

$$J(\mathbf{o}) = \sum_f \left[\frac{|\tilde{\mathbf{h}}(f)\tilde{\mathbf{o}}(f) - \tilde{\mathbf{i}}(f)|^2}{\mathrm{PSD}_n(f)} + \frac{|\tilde{\mathbf{o}}(f) - \tilde{\mathbf{o}}_\mathbf{m}(f)|^2}{\mathrm{PSD}_o(f)} \right], \tag{13}$$

where the tilde denotes the two-dimensional DFT and f is the spatial frequency. The MAP estimation with *a priori* Gaussian statistics for the object therefore leads to a regularized quadratic criterion. Note that the regularizing function is directly related to the object PSD. Furthermore, since the criterion is directly derived from the probability distributions there is no scaling factor (regularization parameter) to be adjusted between the likelihood term and the regularization term.

In this particular case in which the PSF is known and a positivity constraint is not used, an analytical expression of the MAP estimator is obtained by computation of the derivative of the criterion with respect to the object. In Fourier space, it reads

$$\begin{aligned}\tilde{\hat{\mathbf{o}}}_w(f) = &\frac{\tilde{\mathbf{h}}^*(f)\tilde{\mathbf{i}}(f)}{|\tilde{\mathbf{h}}(f)|^2 + \dfrac{\mathrm{PSD}_n(f)}{\mathrm{PSD}_o(f)}} \\ &+ \frac{\dfrac{\mathrm{PSD}_n(f)}{\mathrm{PSD}_o(\mathrm{f})}}{|\tilde{\mathbf{h}}(f)|^2 + \dfrac{\mathrm{PSD}_n(f)}{\mathrm{PSD}_o(f)}}\, \tilde{\mathbf{o}}_\mathbf{m}(f).\end{aligned} \tag{14}$$

This is the expression of the Wiener filter for the special case in which $\mathbf{o_m}$ is not zero.[25] A geometric interpretation of this equation is that, at each frequency, the component of the solution lies on the segment between an ultrarough solution (the inverse filter) and an ultrasmooth solution (the *a priori* mean object); the position on the segment is a function of the signal-to-noise ratio. Note that the introduction of such a nonzero mean for the object does not improve the restoration quality very much because $\mathbf{o_m}$ is typically very slowly varying (that is, not far from being flat), and the signal-to-noise ratio is high at low frequencies. Yet the introduction of a nonzero mean for the PSF will be useful in the myopic extension of the current estimator, because the average PSF is far from being flat (see Subsection 4.B).

The solution given in Eq. (14) is the expected one since, as mentioned in Section 3, in the case of Gaussian statistics, Wiener filtering and the MAP estimation are identical. However, the advantage of the MAP approach is that we can generalize the criterion to the case of myopic deconvolution (see Subsection 4.B).

2. *Possible Estimators with Poisson Statistics*

In astronomical imaging (and in the simulations below), the noise is often predominantly photon noise, which follows Poisson statistics, whereas the estimator given by Eq. (8) has been derived under a Gaussian noise assumption.

One possibility is to derive the true MAP estimator for photon noise statistics. It is obtained when the (quadratic) ML term of the criterion is replaced with the negative log likelihood of the Poisson law, so that Eq. (8) becomes

$$\begin{aligned}J(\mathbf{o}) = &\sum_r (H\mathbf{o})(r) - \mathbf{i}(r)\ln[H\mathbf{o})(r)] \\ &+ (\mathbf{o} - \mathbf{o_m})^t R_o^{-1}(\mathbf{o} - \mathbf{o_m}).\end{aligned} \tag{15}$$

The solution to the minimization of this criterion is no longer analytical and must be sought by a numerical method. A further refinement of this criterion could be to use a mixed Poisson–Gauss noise model to account for both photon and electronic noises.[26]

Another possibility is to still use the estimator given by Eq. (8) [or equivalently by Eq. (13) or Eq. (14)] with R_n equal to a scaled identity matrix, i.e., $\mathrm{PSD}_n(f) = N_{\mathrm{ph}}$, where N_{ph} is the average total flux. Indeed, stationary white Gaussian noise, with a uniform variance equal to the mean number of photons per pixel, is a first approximation of photon noise in the case of a bright and rather extended object. Because of this approximation of the noise statistics, the estimator is no longer a true MAP estimator, and can be termed a regularized least-squares (RLS) estimator.

Yet, for simplicity, we use this RLS estimator below. Indeed, because our aim in this paper is to introduce a myopic deconvolution scheme, we wish to focus on the regularization terms for the object and for the PSF (Subsections 4.A.3 and 4.B) rather than on the noise term. Besides, even if our estimator is suboptimal, it leads to well-restored objects, as is shown in the following subsections.

3. *Choice of the Regularization Function*

The *a priori* information required on the object for computing the regularization function [second term of Eqs. (13) and (15)] consists of two quantities: the mean object and the object PSD. With an ergodicity assumption for the object, $\mathbf{o_m}$ can be estimated by a local average of the image (because the image is itself a kind of local average of the object), the support of this averaging filter being at least the effective support of the PSF (and more if the image is noisy). So this mean object is essentially low frequency.

At high frequencies, the action of the regularization function is to draw the estimate toward zero,

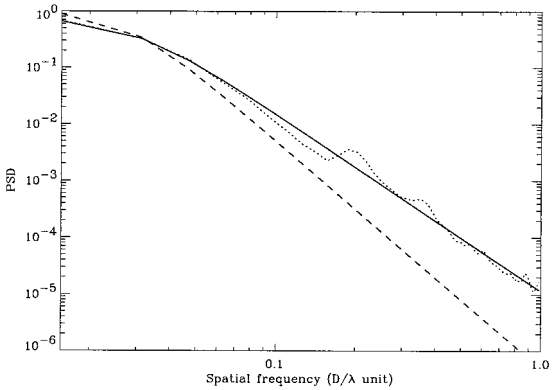

Fig. 3. Normalized PSD models versus spatial frequency: adequate model corresponding to the true object (solid curve), and -4th power-law model corresponding to the Laplacian-type regularization (dashed curve). The square modulus of the true-object Fourier transform (circular average) is shown for comparison (dotted curve). The spatial frequency is normalized to the telescope cutoff frequency. The mean object is assumed here to be constant.

with a stiffness determined by the model taken for the object PSD. As mentioned above, a classical regularization term used in deterministic methods is the square norm of the Laplacian of the object.[18,21] In the Fourier domain it reads $\lambda \sum_f f^4 |\tilde{\mathbf{o}}(f)|^2$. By identification with the second term of Eq. (13), this regularization can be interpreted[17] as a zero-mean Gaussian *a priori* on the object with $\mathrm{PSD}_o(f) \propto f^{-4}$. Besides the fact that the mean should not be taken as equal to zero, this kind of PSD is not appropriate for astronomical objects. The spectrum of typical objects effectively follows a power law at high frequencies, for example, f^{-3} for a uniform disk and between f^{-2} and f^{-4} (depending on the considered direction) for a square. Yet this power, which is denoted hereafter by p and characterizes the regularity of the object, is smaller than 4 even for extremely extended objects such as the Earth viewed from a satellite,[27] and typically is between 2 and 4. The other difficulty with a Laplacian-type regularization term is how to adjust the regularization parameter λ.

We thus choose the following PSD model (see, e.g., Ref. 27 and references therein, and Ref. 28):

$$\begin{aligned}\mathrm{PSD}_o(f) &= E[|\tilde{\mathbf{o}}(f)|^2] - |\tilde{\mathbf{o}}_{\mathbf{m}}(f)|^2 \\ &= N_{\mathrm{ph}}^2/[1 + (f/f_0)^p] - |\tilde{\mathbf{o}}_{\mathbf{m}}(f)|^2, \qquad (16)\end{aligned}$$

where f_0 is a cutoff frequency introduced to avoid the divergence at the origin and is taken as the inverse of the characteristic size of the object. This simple parametric model avoids the need for a hyperparameter estimation; the estimation of a somewhat arbitrary hyperparameter is replaced with that of N_{ph} and f_0 (and p), but these parameters are more physically meaningful. Additionally, in order to check the validity of this model, we have verified, in the restorations presented below, that increasing or decreasing PSD_o by a factor of 10 indeed degrades the restored image.

The validity of such a PSD model is illustrated in Fig. 3. The circular average of the square modulus of the DFT of the true object shown in Fig. 2 is drawn and compared with the model with $p = 4$, which is clearly not good for our object. A much better model is obtained with a f^{-3} high-frequency evolution, i.e., $p = 3$. The shoulder of the curve occurs around f_0 ($\approx 0.03D/\lambda$).

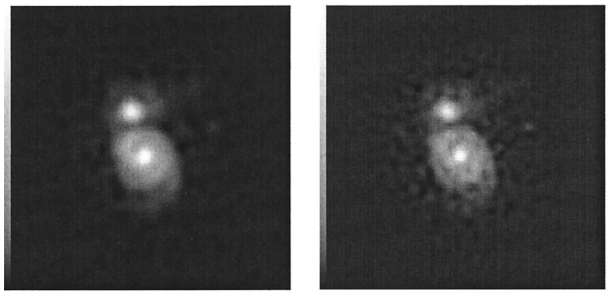

(a) (b)

Fig. 4. Objects restored by classical deconvolution by the RLS estimator with the true PSF, without a positivity constraint: (a) Laplacian-type (f^{-4}) regularization, (b) regularization derived from the good (f^{-3}) object PSD model. The distance to the true object is $d(\hat{\mathbf{o}}, \mathbf{o}) = 63$ for (a) and 56 for (b).

In all the restorations presented below, the input image is the AO-corrected image presented in Fig. 2, normalized to a total flux of 10^6 photons, on which photon noise is added. Figure 4 illustrates the influence of the choice of the object PSD on the quality of the restored object. The results are obtained by application of Eq. (14) (RLS estimator) with the two PSD models shown in Fig. 3. The mean object is taken as the 5×5 local average of the image. The object is better resolved with an f^{-3} PSD fit [Fig. 4(b)] than with the f^{-4} law, which corresponds to a Laplacian-type regularizing function [Fig. 4(a)]. The restoration quality can be quantitatively evaluated by the calculation of a distance to the true object $\mathbf{o}$, defined as

$$d(\hat{\mathbf{o}}, \mathbf{o}) = \left[\frac{1}{N_{\mathrm{pix}}} \sum_{\mathrm{pixels}} |\hat{\mathbf{o}}(r) - \mathbf{o}(r)|^2\right]^{1/2} \text{(photons/pixel)}, \qquad (17)$$

where N_{pix} is the total number of pixels in the image. The distance is indeed larger for the object of Fig. 4 restored with a Laplacian-type regularization: 63, compared with 56 photons obtained with our PSD model. In any case, the distance between the noisy version of Fig. 2 and the true object is much larger (140 photons), which means that the corrected image is not a good estimate of the object and that the estimation is greatly improved by deconvolution.

4. *Addition of a Positivity Constraint*

The object intensity map is a set of positive values, which is important *a priori* information. One should therefore enforce a positivity constraint on the object. This constraint can be implemented in various ways[16]: criterion minimization under the positivity

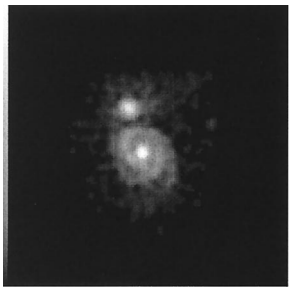

Fig. 5. Object restored by classical deconvolution by the RLS estimator with the true PSF and a positivity constraint. The regularization is derived from the f^{-3} PSD model. The distance to the true object is $d(\hat{\mathbf{o}}, \mathbf{o}) = 53$.

constraint, reparameterization[29] of the object, or explicit modification of the *a priori* probability distribution (e.g., addition of an entropic term). The first two methods can actually be interpreted as an implicit modification of the *a priori* distribution that sets a zero probability to objects that have negative pixel values.

The results presented below are obtained with the RLS estimator and the reparameterization method: We perform a minimization of the criterion given in Eq. (13) with respect to $\mathbf{a}(r)$, defined by $\mathbf{o}(r) = \mathbf{a}(r)^2$. In this case the estimator is not a linear filter and it is not possible to find an analytical solution. The criterion is thus minimized by a numerical iterative algorithm (a conjugate gradient in our case[29]).

Figure 5 shows the gain brought by the positivity constraint when the image shown in Fig. 2 is restored by the RLS estimator. The object is regularized with the f^{-3} PSD model presented in Fig. 3. The distance to the true object is 53 photons, which confirms that the object is better restored with the positivity constraint [compare with Fig. 4(b)].

B. Myopic Deconvolution

The estimation of the long-exposure PSF in astronomical imaging with AO is a difficult subject.[10,30,31] The usual way to obtain the PSF is by calibration on a reference star near the observed object. This method is not satisfactory for several reasons: First, the turbulence is likely to have evolved between the acquisition of the object of interest and that of the reference star. Second, because of the different spatial extents and the different fluxes of the object and the reference star, the control loop is likely to behave differently in the two cases.

Several authors have addressed this problem of deconvolution of turbulence-degraded images with an unknown PSF. Ayers and Dainty[32] used a Gerchberg–Saxton–Papoulis-type algorithm[33–35] and encountered the known[36] convergence problems associated with such projection-based algorithms. Others[37–42] have used methods based on a ML approach, the algorithm used to maximize the likelihood being either the expectation-maximization method[37,39] or the minimization of an explicit criterion.[38,40,41] They have generally recognized the need for a regularization other than the sole positivity (of the object and the PSF) and introduced in particular a bandlimitedness on the PSF.[37,40] This kind of *a priori* information on the solution (and more if it is available) can be introduced naturally if the approach presented above is adopted.

We therefore generalized the deconvolution scheme to the case of myopic deconvolution, in which both the object and the PSF have to be restored.[29] Similarly to what was done for $\mathbf{o}$, the PSF can be considered a stochastic process. Since the PSF can be considered the temporal average of a large number of short-exposure PSF's, its *a priori* statistics can reasonably be assumed to be Gaussian. Following the theoretical developments presented in Subsection 4.A.1, our estimator becomes

$$\begin{aligned}[\hat{\mathbf{o}}, \hat{\mathbf{h}}] &= \arg\max_{\mathbf{o},\,\mathbf{h}} p(\mathbf{o}, \mathbf{h}|\mathbf{i}) \\ &= \arg\max_{\mathbf{o},\,\mathbf{h}} p(\mathbf{i}|\mathbf{o}, \mathbf{h}|)p(\mathbf{o})p(\mathbf{h}) \\ &= \arg\min_{\mathbf{o},\,\mathbf{h}} J(\mathbf{o}, \mathbf{h}) \end{aligned} \tag{18}$$

with a new criterion $J(\mathbf{o}, \mathbf{h})$, which is now a function of $\mathbf{o}$ and $\mathbf{h}$. This criterion has three terms: One is the opposite of the log likelihood of the data, one is an object regularization term, and one is a PSF regularization term, similar to a recently suggested deterministic approach.[43] For stationary Gaussian noise, this criterion can be written as

$$J(\mathbf{o}, \mathbf{h}) = \sum_f \left[\frac{|\tilde{\mathbf{h}}(f)\tilde{\mathbf{o}}(f) - \tilde{\mathbf{i}}(f)|^2}{\mathrm{PSD}_n(f)} + \frac{|\tilde{\mathbf{o}}(f) - \tilde{\mathbf{o}}_{\mathbf{m}}(f)|^2}{\mathrm{PSD}_o(f)} + \frac{|\tilde{\mathbf{h}}(f) - \tilde{\mathbf{h}}_{\mathbf{m}}(f)|^2}{\mathrm{PSD}_h(f)} \right], \tag{19}$$

where PSD_h is the spatial PSD of the PSF, and $\tilde{\mathbf{h}}_{\mathbf{m}}$ is the ensemble mean OTF (Fourier transform of the ensemble mean PSF). Again, when the noise is not Gaussian (which is the case in astronomical imaging), this estimator is not a true MAP estimator but a myopic RLS estimator, unless the first term of the criterion is replaced with the log probability of the noise.

The last term (regularization on the PSF) cannot be ignored, otherwise the myopic deconvolution usually leads to the trivial solution: a Dirac function for the PSF and an object equal to the image. PSD_h is expressed simply as a function of the first two moments of the OTF:

$$\mathrm{PSD}_h(f) = E[|\tilde{\mathbf{h}}(f) - \tilde{\mathbf{h}}_{\mathbf{m}}(f)|^2] = E[|\tilde{\mathbf{h}}(f)|^2] - |\tilde{\mathbf{h}}_{\mathbf{m}}(f)|^2. \tag{20}$$

It should be noted that $\mathrm{PSD}_h(f)$ is zero above the cutoff of the telescope, so that the regularization in particular enforces a zero value for the estimation of $\tilde{\mathbf{h}}(f)$ above the cutoff. Also, if the variations of the

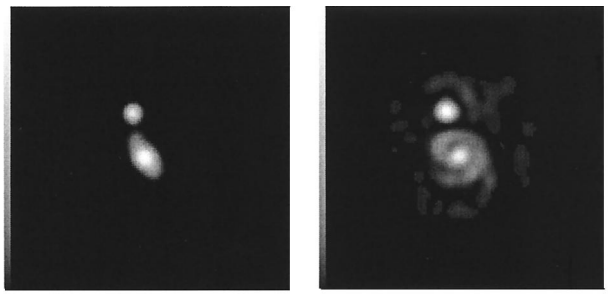

(a) (b)

Fig. 6. Comparison of (a) classical, (b) myopic deconvolutions. In both cases the image $\mathbf{h_r}$ of a reference star is available, but r_0 is 5 cm for $\mathbf{h_r}$ (it was 10 cm for the image $\mathbf{i}$). In (a) the PSF is taken as $\mathbf{h_r}$; in (b) the mean PSF is taken as the circular average of $\mathbf{h_r}$ and PSD_h is taken as the circular average of $|\tilde{\mathbf{h}}_\mathbf{r}|^2$ [see Eq. (23)]. Positivity constraints are applied on the object and the PSF, and the object regularization is derived from the f^{-3} PSD model. The distance to the true object is $d(\hat{\mathbf{o}}, \mathbf{o}) = 442$ in the classical case and 127 in the myopic one.

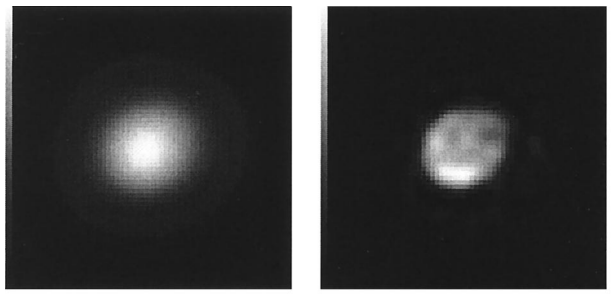

Image (a) Deconvolution (b)

Fig. 7. Observation of the asteroid Vesta with the Office National d'Études et de Recherches AO bench (7 June 1996, 20:58UT): (a) corrected image (estimated Strehl ratio 0.09), (b) object restored by myopic deconvolution with positivity constraint and regularization on both the object and the PSF. The imaging wavelength is 0.7 μm (40-nm spectral bandwidth) with a 5-min exposure time. The estimated number of detected photons is 3.46×10^7. The field of view for the figure is 1.65 arc sec (the image presented here is the processed image truncated to half its size).

PSF are essentially due to turbulence, it can be shown[10,44,45] that PSD_h is given by

$$\mathrm{PSD}_h(f) = (\tau/T)[\mathrm{STF}_\mathbf{m}(f) - |\tilde{\mathbf{h}}_\mathbf{m}(f)|^2], \qquad (21)$$

where $\mathrm{STF}_\mathbf{m}$ is the so-called speckle transfer function (second moment of the short-exposure OTF), τ is the coherence time of the turbulence, and T is the integration time.

The restoration quality obtained with myopic deconvolution is of course related to the quality of the mean PSF $\mathbf{h_m}$ and the PSD model PSD_h. The PSD of the PSF can be viewed as a per-frequency variance of the fluctuations of the OTF around its mean value. Ideally, both $\mathbf{h_m}$ and PSD_h should be estimated from control-loop data.[10,30,31] If these data are not available, $\mathbf{h_m}$ and PSD_h can be approximated by use of the image of a reference star, say $\mathbf{h_r}$. In particular, $\mathbf{h_m}$ can be approximated by the circular average of $\mathbf{h_r}$ if the residual static aberrations of the telescope are known to be negligible, or else by $\mathbf{h_r}$ itself. Similarly, when expected values are replaced with circular averages (over spatial frequencies) in Eq. (20), a possible estimate for PSD_h could be

$$\widehat{\mathrm{PSD}}_h(f) = \langle|\tilde{\mathbf{h}}_\mathbf{r}|^2\rangle(f) - |\langle\tilde{\mathbf{h}}_\mathbf{r}\rangle(f)|^2, \qquad (22)$$

where $\langle\cdot\rangle$ denotes a circular average and the exposure times on the reference star and on the object are assumed to be equal. Yet, because of all the reasons mentioned at the beginning of Subsection 4.B, the true PSF may differ considerably from $\mathbf{h_r}$. That is why we suggest using an estimate of PSD_h higher than this one. In practice, we found that

$$\widehat{\mathrm{PSD}}_h(f) = \langle|\tilde{\mathbf{h}}_\mathbf{r}|^2\rangle(f) \qquad (23)$$

gives satisfactory results. It is an upper bound of Eq. (22) and is a good approximation in the case of a low-quality correction.

Figure 6 shows the effect of the PSF regularization term in the case of a notable variation of the Fried parameter r_0 between the acquisition of the image and that of the reference star; r_0 is assumed to have varied from 10 cm for the image $\mathbf{i}$ to 5 cm for the reference star $\mathbf{h_r}$ (corresponding to a Strehl ratio of 0.01). A classical deconvolution with $\mathbf{h_r}$ as the PSF is compared with the myopic deconvolution with the circular average of $\mathbf{h_r}$ as an estimate of $\mathbf{h_m}$ and the circular average of $|\tilde{\mathbf{h}}_\mathbf{r}|^2$ [see Eq. (23)] as an estimate of PSD_h. In both cases the positivity constraint is enforced on the object and the PSF with the reparameterization proposed in Subsection 4.A.4, and an adequate (f^{-3}) object regularization is used. The distances to the true object are, respectively, 442 and 127 photons. These simulation results prove that a measurement of the PSF, as rough as it may be, can be advantageously used to derive a regularization term, even if it is not reliable enough to be used as an estimate of the kernel in a classical deconvolution.

5. Deconvolution of Experimental Data

The myopic deconvolution scheme is applied here to an experimental image of the asteroid Vesta recorded in June 1996 with the Office National d'Études et de Recherches Aérospatiales AO bench installed on the 1.52-m telescope at the Observatoire de Haute Provence.[46] The system characteristics are identical to the ones taken for the simulation presented in Section 2.

A 128×128 image of Vesta (field of view 3.3 arc sec) was recorded at the imaging wavelength 0.7 μm (40-nm spectral bandwidth). The central part of the image is shown in Fig. 7. The exposure time is 5 min, and the estimated number of detected photons is 3.46×10^7. The asteroid edges are not detected, and no detail can be seen on the surface. The myopic deconvolution scheme described in Subsection 4.B is applied to this image. The positivity constraint is used on both the object and the PSF. The object

PSD is estimated by a polynomial fit of the Fourier-transform square modulus of a uniform disk of diameter 0.9 arc sec. The ensemble mean of the object is taken as the 5×5 local average of the image. The PSD used for the PSF is the circular average of the square modulus of the OTF deduced from the image of an unresolved star of similar magnitude (HR5586 in this case). The restored object is shown in Fig. 7(b). The estimated object exhibits sharp edges. Dark and bright spots are also resolved on the surface. These structures are unlikely to be artifacts; similar features have indeed been observed by astronomers.[47,48] The Strehl ratio computed on the estimated PSF is 0.09.

6. Conclusion

A stochastic framework for the restoration of long-exposure AO images has been presented.

It has been shown that the regularization function is advantageously derived from the PSD of the class of object being observed. Indeed, this leads to better results than does a regularization with a heuristic criterion, and it avoids the need for a hyperparameter estimation, as demonstrated by simulations.

The positivity *a priori* information has been incorporated into the restoration, and its beneficial influence has been shown. This restoration scheme has been extended to the case of imprecise knowledge of the PSF, while all the reduced available information on the PSF (positivity and estimates of the mean and the PSD) is used. Last, this scheme has been successfully applied to experimental data.

Future work should include a better modeling of the noise, with possibly a mixed Poisson–Gauss model to account for both photon and electronic noises. It could also include the refinement of the *a priori* information on the object and the PSF and possibly use a nonstationary nonquadratic object regularization in order to preserve the edges better. Additionally, the PSF mean and the PSD could be estimated from control-loop data rather than from a reference star. Also, our method could be extended to a multiframe myopic deconvolution. Last, the uniqueness of the solution and the existence or not of local minima for the myopic criterion deserve to be studied.

This research was supported by contracts from Direction des Recherches, Etudes et Techniques, Ministère de la Défense, France. The authors thank Eric Thiébaut, Jean-Pierre Véran, Pierre-Yves Madec, and Guy Le Besnerais for many fruitful discussions, as well as Didier Rabaud and all our colleagues who took part in the observing run at the Observatoire de Haute Provence. Thanks also to Isabelle Tallon-Bosc, Michel Tallon, and Christophe Dumas who selected the astronomical objects to be observed during that run.

For further information contact us by email at conan@onera.fr.

References

1. A. Labeyrie, "Attainment of diffraction-limited resolution in large telescopes by Fourier analysing speckle patterns," Astron. Astrophys. **6,** 85–87 (1970).
2. K. T. Knox and B. J. Thompson, "Recovery of images from atmospherically degraded short exposure photographs," Astrophys. J. Lett. **193,** L45–L48 (1974).
3. G. Weigelt, "Modified astronomical speckle interferometry "speckle masking"," Opt. Commun. **21,** 55–59 (1977).
4. J. Primot, G. Rousset, and J.-C. Fontanella, "Deconvolution from wavefront sensing: a new technique for compensating turbulence-degraded images," J. Opt. Soc. Am. A **7,** 1598–1608 (1990).
5. J. W. Hardy, J. E. Lefevbre, and C. L. Koliopoulos, "Real time atmospheric compensation," J. Opt. Soc. Am. **67,** 360–369 (1977).
6. G. Rousset, J.-C. Fontanella, P. Kern, P. Gigan, F. Rigaut, P. Léna, C. Boyer, P. Jagourel, J.-P. Gaffard, and F. Merkle, "First diffraction-limited astronomical images with adaptive optics," Astron. Astrophys. **230,** L29–L32 (1990).
7. F. Rigaut, G. Rousset, P. Kern, J.-C. Fontanella, J.-P. Gaffard, F. Merkle, and P. Léna, "Adaptive optics on a 3.6-m telescope: results and performance," Astron. Astrophys. **250,** 280–290 (1991).
8. M. C. Roggemann and C. L. Matson, "Power spectrum and Fourier phase spectrum estimation by using fully and partially compensating adaptive optics and bispectrum postprocessing," J. Opt. Soc. Am. A **9,** 1525–1535 (1992).
9. J.-M. Conan, P.-Y. Madec, and G. Rousset, "Image formation in adaptive optics partial correction," in *Active and Adaptive Optics*, F. Merkle, ed., Vol. 48 of ESO Conference and Workshop Proceedings (European Southern Observatory, Garching, Germany, 1993), pp. 181–186.
10. J.-M. Conan, "Étude de la correction partielle en optique adaptative," Ph.D. thesis (Université de Paris XI, Orsay, France, 1994).
11. A. K. Jain, *Fundamentals of Digital Image Processing* (Prentice-Hall, Englewood Cliffs, New Jersey, 1989), Chap. 2.
12. D. L. Fried, "Statistics of a geometric representation of wavefront distortion," J. Opt. Soc. Am. **55,** 1427–1435 (1965).
13. A. Tikhonov and V. Arsenin, *Solutions of Ill-Posed Problems* (Winston, Washington, D.C., 1977).
14. M. Z. Nashed, "Operator-theoretic and computational approaches to ill-posed problems with applications to antenna theory," IEEE Trans. Antennas Propag. **AP-29,** 220–231 (1981).
15. W. L. Root, "Ill-posedness and precision in object-field reconstruction problems," J. Opt. Soc. Am. A **4,** 171–179 (1987).
16. D. M. Titterington, "General structure of regularization procedures in image reconstruction," Astron. Astrophys. **144,** 381–387 (1985).
17. G. Demoment, "Image reconstruction and restoration: overview of common estimation structures and problems," IEEE Trans. Acoust. Speech Signal Process. **37,** 2024–2036 (1989).
18. B. R. Hunt, "The application of constrained least squares estimation to image restoration by digital computer," IEEE Trans. Comput. **C-22,** 805–812 (1973).
19. W. H. Richardson, "Bayesian-based iterative method of image restoration," J. Opt. Soc. Am. **62,** 55–59 (1972).
20. L. B. Lucy, "An iterative technique for rectification of observed distributions," Astrophys. J. **79,** 745–754 (1974).
21. D. L. Phillips, "A technique for the numerical solution of certain integral equations of the first kind," J. Assoc. Comput. Mach. **9,** 84–97 (1962).
22. A. K. Katsaggelos, ed., *Digital Image Restoration*, Springer Series in Information Sciences, (Springer-Verlag, Berlin, 1991), Chap. 1.

23. H. L. Van Trees, *Detection, Estimation, and Modulation Theory Part I* (Wiley, New York, 1968).
24. A. Papoulis, *Probability, Random Variables, and Stochastic Processes*, 3rd ed. (McGraw-Hill, New York, 1991).
25. B. R. Hunt, "Bayesian methods in nonlinear digital image restoration," IEEE Trans. Comput. **C-26,** 219–229 (1977).
26. J. Nunez and J. Llacer, "A general Bayesian image reconstruction algorithm with entropy prior: preliminary application to HST data," Publ. Astron. Soc. Pac. **105,** 1192–1208 (1993).
27. A. P. Kattnig and J. Primot, "Model of the second-order statistic of the radiance field of natural scenes, adapted to system conceiving," in *Visual Information Processing* VI, S. K. Park and R. D. Juday, eds., Proc. SPIE **3074,** 132–141 (1997).
28. F. O. Huck, R. Alter-Gartenberg, and Z. Rahman, "Image gathering and digital restoration for fidelity and visual quality," Comput. Vision Graphics Image Process. **53,** 71–84 (1991).
29. E. Thiébaut and J.-M. Conan, "Strict *a priori* constraints for maximum-likelihood blind deconvolution," J. Opt. Soc. Am. A **12,** 485–492 (1995).
30. J.-P. Véran, F. Rigaut, and H. Maître, "Adaptive optics long exposure point spread function retrieval from wavefront sensor measurements," in *Adaptive Optics*, M. Cullum, ed., Vol. 54 of ESO Conference and Workshop Proceedings (European Southern Observatory, Garching, Germany, 1995), pp. 497–502.
31. J.-P. Véran, F. Rigaut, H. Maître, and D. Rouan, "Estimation of the adaptive optics long-exposure point-spread function using control loop data," J. Opt. Soc. Am. A **14,** 3057–3069 (1997).
32. G. R. Ayers and J. C. Dainty, "Iterative blind deconvolution and its applications," Opt. Lett. **13,** 547–549 (1988).
33. R. W. Gerchberg and W. O. Saxton, "A practical algorithm for the determination of phase from image and diffraction plane pictures," Optik **35,** 237–246 (1972).
34. R. W. Gerchberg, "Super-resolution through error energy reduction," Opt. Acta **21,** 709–720 (1974).
35. A. Papoulis, "A new algorithm in spectral analysis and band-limited extrapolation," IEEE Trans. Circuits Syst. **CS-22,** 735 (1975).
36. A. Levi and H. Stark, "Restoration from phase and magnitude by generalized projections," in *Image Recovery: Theory and Application*, H. Stark, ed. (Academic, New York, 1987), Chap. 8, pp. 277–320.
37. T. J. Holmes, "Blind deconvolution of speckle images quantum-limited incoherent imagery: maximum-likelihood approach," J. Opt. Soc. Am. A **9,** 1052–1061 (1992).
38. R. G. Lane, "Blind deconvolution of speckle images," J. Opt. Soc. Am. A **9,** 1508–1514 (1992).
39. T. J. Schultz, "Multiframe blind deconvolution of astronomical images," J. Opt. Soc. Am. A **10,** 1064–1073 (1993).
40. S. M. Jefferies and J. C. Christou, "Restoration of astronomical images by iterative blind deconvolution," Astrophys. J. **415,** 862–874 (1993).
41. R. G. Lane, "Methods for maximum-likelihood deconvolution," J. Opt. Soc. Am. A **13,** 1992–1998 (1996).
42. J. C. Christou, D. Bonaccini, and N. Ageorges, "Deconvolution of adaptive optics near-infrared system (ADONIS) images," in *Adaptive Optics and Applications*, R. K. Tyson and R. Q. Fugate, eds., Proc. SPIE **3126,** 68–80 (1997).
43. Y.-L. You and M. Kaveh, "A regularization approach to joint blur identification and image restoration," IEEE Trans. Image Process. **5,** 416–428 (1996).
44. J. C. Dainty and A. H. Greenaway, "Estimation of spatial power spectra in speckle interferometry," J. Opt. Soc. Am. A **69,** 786–790 (1979).
45. J. W. Goodman, *Statistical Optics* (Wiley-Interscience, New York, 1985), Chap. 8.
46. P. Y. Madec, D. Rabaud, B. Fleury, J. M. Conan, L. Rousset-Rouvière, F. Mendez, J. Montri, V. Michau, G. Rousset, and M. Séchaud, "Essais du banc d'optique adaptative ONERA à l'OHP," Lett. Observatoire de Haute Provence **16,** 2–3 (1997).
47. C. Dumas and O. R. Hainaut, "Mapping Vesta in the visible and near-infrared: the 1994 and 1996 oppositions as viewed from the ground," in *Evolution of Igneous Asteroids: Focus on Vesta and the HED Meteorites*, D. W. Mittlefehldt and J. J. Papike, eds., Lunar and Planetary Institute Tech. Rep. 96-02(1) (Lunar and Planetary Institute, Houston, Tex., 1996), pp. 7–8.
48. C. Dumas and O. R. Hainaut, "Mapping Vesta with adaptive optics: the 1996 opposition," Bull. Am. Astron. Soc. **28,** 1101 (1996).